J Mater Sci: Mater Med (2009) 20:1039–1046
DOI 10.1007/s10856-008-3674-0

Preparation of highly porous hydroxyapatite from cuttlefish bone

H. Ivankovic · G. Gallego Ferrer · E. Tkalcec · S. Orlic · M. Ivankovic

Received: 30 September 2008 / Accepted: 15 December 2008 / Published online: 10 January 2009

Abstract Hydroxyapatite structures for tissue engineering applications have been produced by hydrothermal (HT) treatment of aragonite in the form of cuttlefish bone at 200°C. Aragonite ($CaCO_3$) monoliths were completely transformed into hydroxyapatite after 48 h of HT treatment. The substitution of CO_3^{2-} groups predominantly into the PO_4^{3-} sites of the $Ca_{10}(PO_4)_6(OH)_2$ structure was suggested by FT-IR spectroscopy and Rietveld structure refinement. The intensity of the $\nu_3PO_4^{3-}$ bands increase, while the intensity of the $\nu_2CO_3^{2-}$ bands decrease with the duration of HT treatment resulting in the formation of carbonate incorporating hydroxyapatite. The SEM micrographs have shown that the interconnected hollow structure with pillars connecting parallel lamellae in cuttlefish bone is maintained after conversion. Specific surface area (S_{BET}) and total pore volume increased and mean pore size decreased by HT treatment.

1 Introduction

Hydroxyapatite (HAP; $Ca_{10}(PO_4)_6(OH)_2$) due to its similarity with the mineral phase of bone has been studied for many years as an implant material [1]. In recent years, particular attention has been paid to the synthesis of HAP ceramics with the porous morphology required for vascularization, bone cell invasion, and angiogenesis, which further improve its biomedical properties [2]. The HAP structure can incorporate a wide variety of ions implying a variable defect structure of HAP. In biological apatites, or apatites originating from biogenetic materials, the presence of other mineral ions, such as Na^+, K^+, Mg^{2+}, F^- as well as substitution of carbonate ions into the HAP structure is very common [3]. The carbonate ion substitutes either at the phosphate tetrahedron (B-type substitution) or at the hydroxyl site (A-type substitution) [4]. The biological apatite that constitutes bone mineral is considered to be of mixed AB-type substitution [5]. Of particular importance is the carbonate substitution for the phosphate ion (B-type substitution), because there exists the correlation between the concentration of incorporated carbonate ion and physical properties of B-type carbonate HAP [6]. Recent experimental and theoretical publications address the controversial subjects of the carbonate substitution in HAP structure. It is generally agreed that the planar carbonate ion substitutes for the phosphate tetrahedron in the B-type structure, however, the exact arrangement of the carbonate in the structure is still unresolved [6].

While synthetic materials have been widely used in the biomedical field with great success, natural structural materials are now providing an abundant source of novel biomedical applications [7]. During the last decade, an increased understanding of biomineralization has initiated improvements in biomimetic synthesis methods and production of new generation of biomaterials. The use of natural biogenic structures and materials such as corals [7, 8], seashells [9], animal bones [10], etc., for medical purposes has been motivated by limitations in generating synthetic materials with the requisite structure and mechanical integrity. Since 1970s it is well-known that if the bioceramic prosthesis with appropriate interconnected

H. Ivankovic (✉) · E. Tkalcec · S. Orlic · M. Ivankovic
Faculty of Chemical Engineering and Technology, University of Zagreb, Zagreb, Croatia
e-mail: hivan@fkit.hr

G. Gallego Ferrer
Centro de Biomateriales, Universidad Politecnica de Valencia, Valencia, Spain

pores is used, hard and soft tissue will grow into the surface of pores and bond will be produced. The hydrothermal transformation of corals into HAP was first used by Roy and Linnehan [11] in 1974. They reported that complete replacement of aragonite by phosphates was achieved at 270°C and 103 MPa. HAP derived from Indian corals using hydrothermal process was reported by Sivakumar et al. [12]. Hydrothermal conversion of Australian corals into HAP was studied by Hu, [7] and Kasperk and Ewers [13] prepared HAP from calcified algae in 1986. HAP was first synthesized from the mineral component of cuttlefish bone via hydrothermal transformation in 2005 [14] and there are only a few papers dealing with this natural aragonite [14, 15]. Studies carried out by Rocha et al. [14, 15] indicated that aragonite completely transformed after 24 h at 200°C forming AB-type carbonate apatite, retaining the overall microstructure and skeleton architecture of aragonite in the cuttlefish bones.

The aim of the present work, was to study the hydrothermal conversion of aragonite (calcium carbonate) of cuttlefish bones (*Sepia officinalis* L.) from Adriatic Sea. The major concern was to quantify carbonate in the transformed HAP formed by heat-treatment at 200°C for various times (1–48 h) using FT-IR analysis and XRD Rietveld structure refinement of HAP. Microstructure and retained skeleton architecture of formed HAP ceramic was studied by scanning electron microscopy.

2 Materials and experimental procedure

Dry cuttlefish bone (*Sepia officinalis* L.) from Adriatic Sea was cut into small pieces about 2 cm^3 large and was first heated to 350°C for 3 h to remove the organic component, and then sealed with the 15 ml aqueous solution of 0.6 M $NH_4H_2PO_4$ in Teflon lined stainless steel pressure vessel at 200°C for various times (1–48 h). The stoichiometrically required aqueous solution of $NH_4H_2PO_4$ to set the ratio Ca/P = 1.67 was determined using the data of DSC and TG analysis of raw cuttlefish bones. The formed HAP was washed with boiling water and dried at 110°C. The porosity studies of cuttlefish bones were carried out through the use of Hg intrusion porosimeter Carlo Erba 2000 WS. Pieces of cuttlefish bones about 1 g in weight were loaded in a penetrometer cell and evacuated, and then filled with mercury under pressure. The volume of the mercury that intruded was measured as a function of pressure. The quantification of meso and microporosity was carried out according to the Brunauer–Emmett–Teller method by nitrogen adsorption–desorption isotherms at liquid N_2 temperature on a Micromeretics ASAP 2000 instrument. The mean pore size was estimated from the desorption branch of the nitrogen adsorption–desorption isotherms by the Barrett–Joyner–Halenda (BJH) method. The conversion of aragonite into HAP was followed by X-ray diffraction analysis (Philips PW 1820 counter diffractometer with Cu$K\alpha$ radiation), scanned in the range of diffraction angles between 10 and 120° with a 2θ step of 0.02°/10 s. Identification of the phases was performed by comparing the experimental XRD patterns to standards compiled by the Joint Committee on Powder Diffraction Standards (JCPDS) using the cards 41-1475 for aragonite, 47-1473 for calcite, and 09-432 for HAP. The Rietveld structure refinement [16] was carried out using a program TOPAS 2.1 (Bruker AXS) [17]. The structure of Holly Springs HAP was used as a starting model without inclusion of CO_3^{2-} ions in the structure. The background was modeled with six Chebyshev polynomials. The peak profiles were fitted with PV-TCHZ pseudo Voigt (Thomson Cost Hasting pseudo Voigt) function. Unit cell parameters, positional parameters (except H), and finally occupancies were all varied. Preferred orientation parameter was also allowed to vary, but the coefficients indicated very little preferred orientation in the samples. The Ca1 occupancy was fixed to 1.0 and isotropic displacement parameters were held constant at those of Holly Springs HAP [18]. In the samples HT-treated at 200°C for 4, 8, and 24 h, aragonite was not completely transformed and was allowed to vary simultaneously with HAP. The amount of CO_3^{2-} incorporated in the structure of HAP was deduced indirectly under the constraints that the sum of PO_4^{3-} and CO_3^{2-} per phosphate site was one with six sites per unit cell. Fourier transform infrared spectra (FT-IR) were performed by attenuated total reflectance (ATR) spectroscopy for solids with a diamond crystal. Simultaneous differential thermal analysis (used in DSC mode) and thermogravimetry (DSC-TGA) was carried out to determine the amount of $CaCO_3$ in cuttlefish bones on Netzsch STA 409 with the constant synthetic air flow of 30 cm^3 min^{-1} and at the heating rate of 10 K min^{-1}. The microstructure of heated (350°C) and HT-treated cuttlefish bones have been examined by scanning electron microscopy (SEM ISIDS-130).

3 Results and discussion

3.1 Differential thermal analysis and thermogravimetry of raw and heat-treated cuttlefish bone

Differential thermal analysis and thermogravimetry of raw cuttlefish bone and that heat-treated at 350°C are shown in Fig. 1. The organic content in raw cuttlefish bone is shown on DSC scans as a weak exothermic peak with the maximum at 320°C, and the decomposition of inorganic part of cuttlefish bone, i.e., aragonite, is shown as the endothermic effect with minimum at 735°C. The small amount of calcite

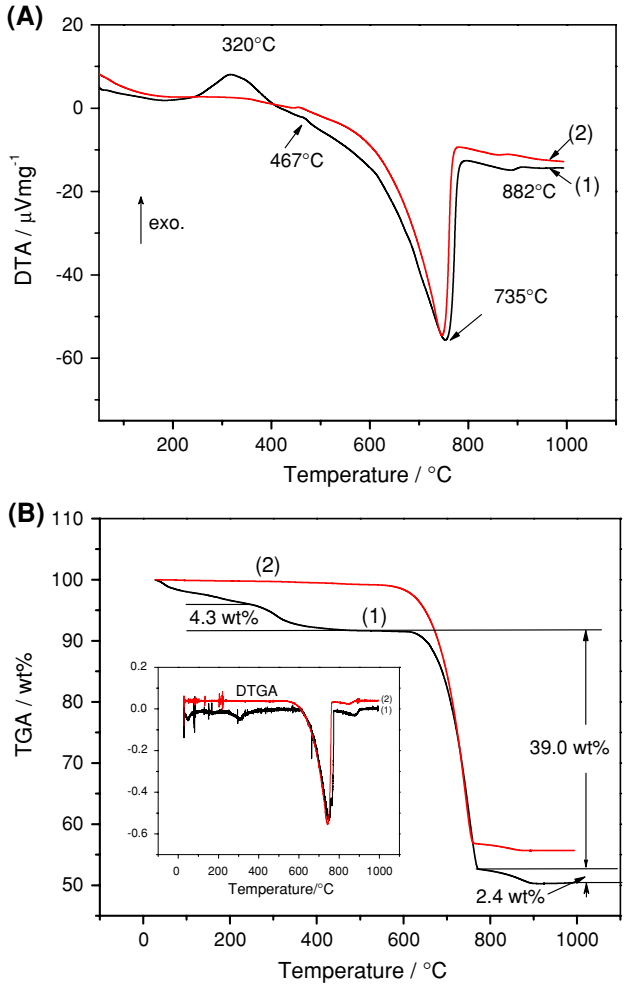

Fig. 1 **a** Differential thermal analysis, **b** thermogravimetry of raw and heat-treated cuttlefish bone; (1) raw bone, (2) heat-treated at 350°C for 3 h

led to an endothermic trough at 882°C. The weight loss on TGA scan (Fig. 1b) between 236 and 436°C due to the burning of the organics was 4.3 wt.%, while the weight loss between 567°C and 895°C was 39.0 wt.% and is attributed to the decomposition of aragonite. On DSC, TGA, and derivative of TGA (DTGA) scans small effect attributed to calcite was also noticed. A difference in the amount of calcite present was observed from sample to sample, a result of the bone coming from different positions within the cuttlefish. Small but noticeable exothermic peak at 467°C was indicated in the raw as well as in the heat-treated cuttlefish bone, which is not accompanied by any weight loss. Rocha et al. [14] have found small exothermic peak but at somewhat lower temperature (430°C) and have attributed it to thermally induced transformation of metastable aragonite into calcite. The metastable transformation of aragonite into calcite could be the cause of the appearance of small exothermic peak, however, the peak position depends most probable on bone origin.

XRD analysis indicated that the dorsal shield and the lamellae matrix of raw cuttlefish bone consist exclusively of aragonite. In the boundaries of dorsal shield and lamellae matrix a thick organic material is placed (Fig. 2), which looks like a small "shirt" enveloped around dorsal shield [19]. The organic "shirt" made it possible to separate thoroughly the heat-treated dorsal shield from the matrix lamellae. However, after the heat-treatment at 350°C aragonite in the dorsal shield partially transforms into calcite, as shown in XRD patterns. On the contrary, the lamellae matrix do not transforms by the heat-treatment at 350°C. We suppose that the transformation of aragonite into calcite was accelerated in the dorsal shield as it is the most external part the cuttlefish bone, and more exposed to oxidative environment during the heat-treatment, than the lamellae matrix.

3.2 Characterization of biogenic aragonite and hydrothermally transformed HAP

The porosity, specific surface area, mean pore size, and total pore volume of raw cuttlefish bones and converted HAP at 200°C for 48 h are shown in Table 1. The porosity of the raw cuttlefish bone yields 90%, which is in agreement with the literature [19], and the specific surface area,

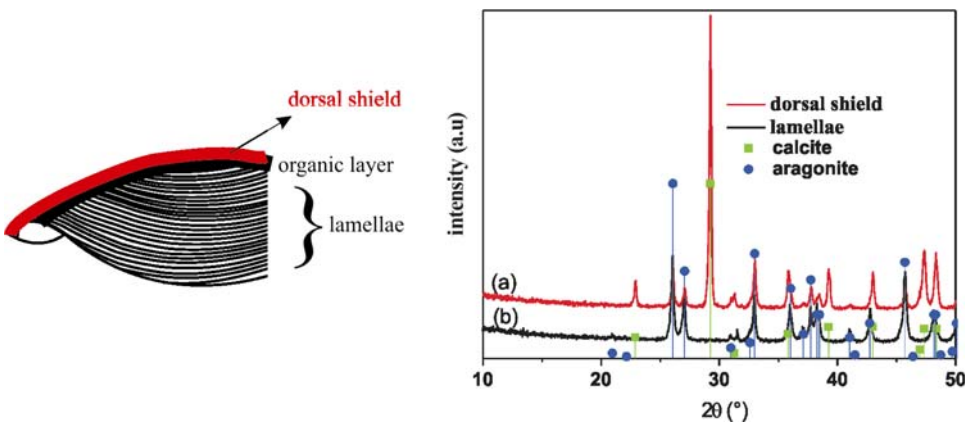

Fig. 2 A part of transverse section through cuttlefish bone and XRD pattern of inorganic part of its dorsal shield (**a**) and the lamellae matrix (**b**) heat-treated at 350°C for 3 hours

Table 1 Porosity, specific surface area, S_{BET}, mean pore size, and total pore volume of raw cuttlefish bone and hydrothermally converted HA

Cuttlefish bone	Porosity (%)	S_{BET} ($m^2\ g^{-1}$)	Mean pore size (nm)	Total pore volume[a] (cm^3/g)
Raw	90	2.5	20	0.0134
Heated at 350°C	96	3.1	24.4	0.0208
HAP 200°C/48 h	94	8.5	21	0.0525

[a] Estimated using BJH desorption branch of the isotherms

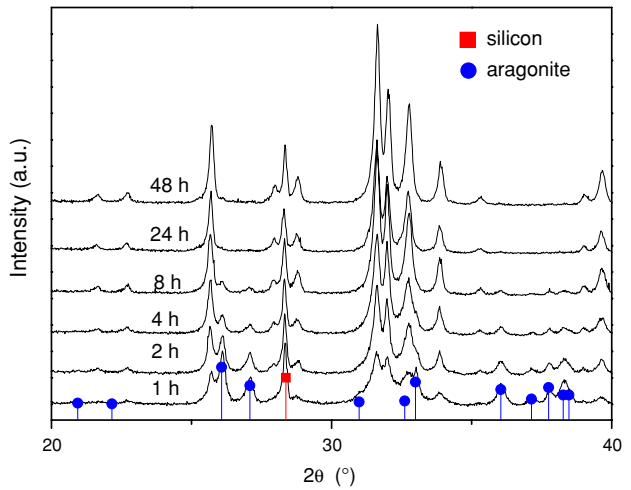

Fig. 3 XRD patterns of hydrothermally (HT) converted HAP at various times (1–48 h). The vertical lines are the 2θ positions of aragonite (JCPDS 41-1475) and calcite (JCPDS 47-1473). For purpose of clarity, the HAP lines (JCPDS 09-432) were not marked

S_{BET}, of raw material is 2.5 $m^2\ g^{-1}$. When the organic component is removed by heating at 350°C the porosity increases to about 96%, and the S_{BET} increases to 3.1 $m^2\ g^{-1}$. After hydrothermal transformation into HAP the porosity somewhat decreases to about 94%, and the specific surface area further increases to 8.5 $m^2\ g^{-1}$. The total pore volume increases, while the mean pore size does not change significantly.

3.3 X-ray studies and FT-IR analysis

The conversion of aragonite into HAP was followed by XRD analysis (Fig. 3) and FT-IR spectroscopy (Fig. 4). The raw cuttlefish bone comprises pure aragonite which gradually converts into HAP by treatment with $NH_4H_2PO_4$ under hydrothermal condition described above. The content of untransformed aragonite together with the crystallite size and unit cell parameters of the synthesized HAP and Holly Springs [20] are given in Table 2. Gibson et al. [6],

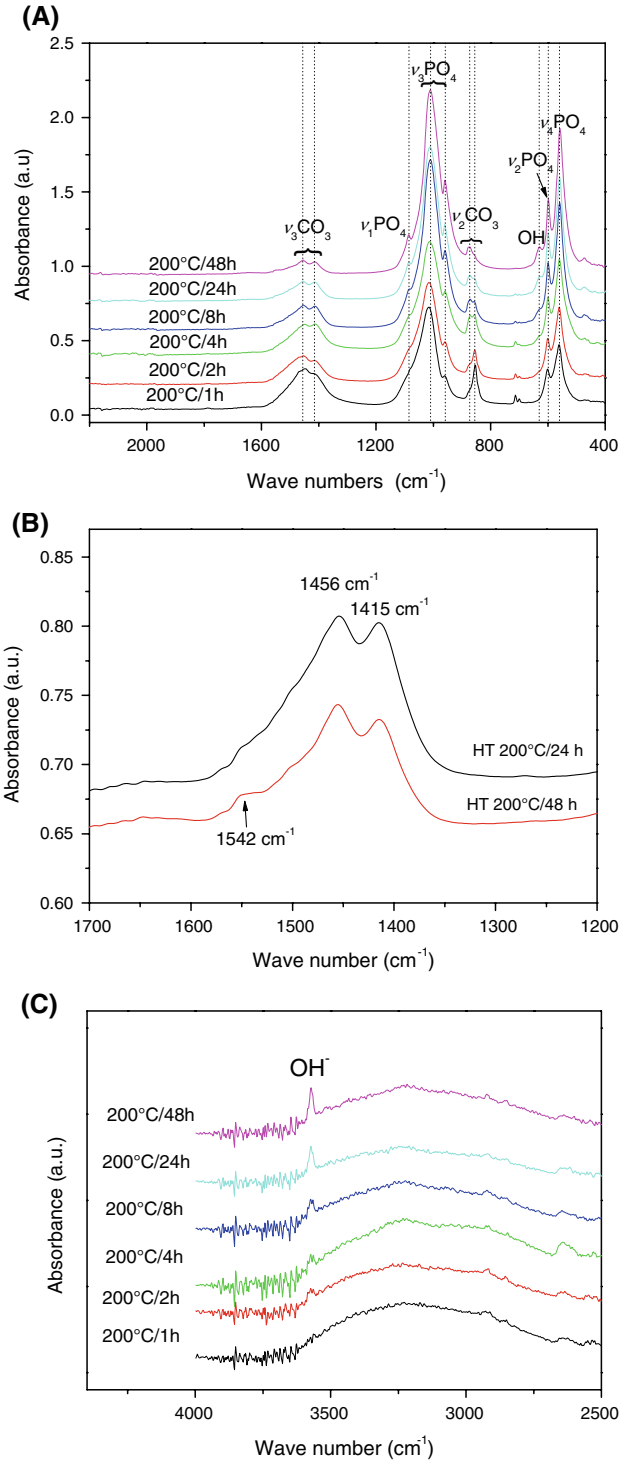

Fig. 4 **a** FT-IR spectra of cuttlefish bone heated at 350°C and hydrothermally transformed in HAP at various conditions. **b** FT-IR spectra of CO_3^{2-} bands at 1,420 and 1,446 cm^{-1} with the shoulder at 1,485 cm^{-1}. Notice the absence of A-type carbonated hydroxyapatite in ~1,540 cm^{-1} region for all samples except for the sample heat-treated at 200°C for 48 h. **c** FT-IR spectra of OH^- stretching vibrations

Table 2 Unit cell parameters, crystallite size, and aragonite content in hydrothermally treated samples

	200°C/4 h	200°C/8 h	200°C/24 h	200°C/48 h	Holly Springs single crystal
a (Å)	9.4369(3)	9.4247(3)	9.4255(3)	9.4284(3)	9.4240(3)
c (Å)	6.9017(3)	6.8981(3)	6.8893(3)	6.8914(3)	6.8790(3)
Crystallite size (nm)	37.4(5)	63(1)	68(2)	64(2)	–
c/a	0.7313	0.7319	0.7309	0.7309	0.7299
Aragonite content (wt%)	17.2(3)	9.7(3)	1.2(2)	–	n.d.

Standard deviations are given in brackets

studying the synthesis of carbonate-substituted HAP (AB-type), have found that the *a*-axis decreases and *c*-axis increases with the increasing amount of incorporated carbonate group into HAP structure. The same behavior of unit cell parameters, as a consequence of the incorporation of CO_3^{2-} group into HAP structure, was observed by Chakraborty [21]. In this work, the samples HT-treated for 8 h and longer show just opposite trend, i.e., the *a*-axis increases and *c*-axis decreases with duration of HT treatment. This can be explained with the decreased amount of carbonate groups incorporated into the HAP structure, as it is confirmed by FT-IR spectra. However, the sample HT-treated for 4 h, probably because of lower crystallinity (crystallite size ~37 nm) and a defective arrangement of the HAP structure exhibited unexpectedly higher values for both *a*- and *c*-axes of the unit cell. The examination of cell dimensions of the prepared samples reveals that, in comparison with the Holly Springs HAP, there is an elongation in the *a*- and *c*-axes. Considering that the elongation occurs in both axes it has to be assumed that the changes in the carbonate and phosphate substitution occur simultaneously during HT treatment. Quantitative XRD analysis of the sample HT-treated at 200°C for 4 h yielded ~17.2 wt.% of aragonite, and HT treatment for 8 h diminished aragonite to ~9.7 wt.%. The sample HT-treated for 24 h showed small amount of aragonite (1.2 wt.%) while the sample HT-treated for 48 h exhibited no other crystalline phases but HAP. The *c/a* ratios agree with the corresponding values obtained by Chakraborty [21] for human bone specimens. Final atomic coordinates, occupancy factors, and agreement factors are given in Table 3. Some authors [21] assumed that the C replaces the P in the *6h* positions. As the controversy exists concerning the exact configuration of the carbonate substitution in the lattice of B-type carbonate HAP [6], we used the model without explicit inclusion of CO_3^{2-} in *6h* position, and the sum of the occupancy factors P and C constrained to unity. The Rietveld refinement confirmed that Ca is essentially fully occupied. On the other hand, the occupancies of P and O3 are significantly less than unity and are consistent with the substitution of the phosphate group by the carbonate ion. The P occupancy increases with the time of HT treatment, which is in agreement with the intensity ratios of $\nu_3PO_4^{3-}$/$\nu_2CO_3^{2-}$ bands of IR spectra (see later in Fig. 6). Unit cell contents from Rietveld analysis are given in Table 4. The molar ratio of Ca/P ranges between 1.83 and 1.89 which is higher than the stoichiometrical value (1.67) indicating the presence of carbonate in the structure and consequently the deficiency of phosphate in the structure. The formula given by the unit cell contents for samples 200°C/48 h (which contains no aragonite) is

$$Ca1_4Ca2_{5.999}(PO_4)_{5.455}(CO_3)_{0.545}(OH)_{2.54}$$

where, the OH^- ion content is that derived by the requirement for charge balance.

FT-IR spectra of samples are given in Fig. 4. In the spectrum of the cuttlefish bone HT-treated at 200°C for 1 h (except of vibration bands due to aragonite at 1,446 cm^{-1}(ν_3); 1,082.9 (ν_1); 856.8 (ν_2); and doublet at 712.8 and 699.6 cm^{-1}(ν_4) [22]) the appearance of the bands of HAP assigned to PO_4^{3-} groups [23] (ν_3, 1,085 and 1,010 cm^{-1}; ν_1, 960 cm^{-1}; ν_4, 558 and 597 cm^{-1}; and ν_2, 473 cm^{-1}) are observed. There are two types of carbonate substitution in HAP. The carbonate substitute either at the phosphate tetrahedral sites (B-type) or at the hydroxyl sites (A-type) or both (AB-type) [24, 25]. Careful analysis of spectra indicates that CO_3^{2-} groups are preferentially incorporated on tetrahedral PO_4^{3-} sites as suggested by the vibration frequencies of CO_3^{2-} at 872 cm^{-1} for ν_2, and at 1,454 and 1,414 cm^{-1} for ν_3 bands. The lower intensity band for $\nu_2CO_3^{2-}$ at 880 cm^{-1} and $\nu_3CO_3^{2-}$ band centered at 1,540 cm^{-1} are characteristic for the A-type substitution [24]. The presence of small amount of the A-type substituted HAP is suggested by the very weak band at 1,540 cm^{-1} seen in the sample HT-treated at 200°C for 48 h (Fig. 4b). The B-type substitution is dominant in the HT-treated samples. The intensity of $\nu_2CO_3^{2-}$ band at 872 cm^{-1} decreases, and those of $\nu_3PO_4^{3-}$ bands increases with the time of HT treatment. Accordingly, the intensity ratio of $\nu_3PO_4^{3-}$/$\nu_2CO_3^{2-}$ also increases with the duration of HT treatment, as seen in Fig. 5. That is in agreement with the decrease of the CO_3^{2-} incorporation with hydrothermal treatment time obtained by Rietveld structure refinement, as seen in Table 4. The stretching (3,565 cm^{-1}) and librational (633 cm^{-1}) modes of the OH^- groups are absent in the samples HT-treated for 1 h,

Table 3 Final atomic coordinates, occupation factors and agreement factors for samples hydrothermally treated for various times

Sample	R_{exp}	R_{wp}	R_p	Gof	Atom	Wyc.	Occ.	*x*	*y*	*z*
200°C/4 h	9.45	12.85	8.13	1.55	O1	6	0.96(1)	0.332(1)	0.479(1)	0.25
					O2	6	0.97(1)	0.580(1)	0.460(1)	0.25
					O3	12	0.86(1)	0.342(1)	0.258(1)	0.0739(1)
					P1	6	0.89(1)	0.3955(7)	3.3687(6)	0.25
					Ca1	4	1	0.3333	0.6666	0.0012(6)
					Ca2	6	1.004(8)	0.2437(5)	0.9859(5)	0.25
					O(H)	4	0.57(1)	0	0	0.166(2)
200°C/8 h	8.73	12.02	8.13	1.48	O1	6	0.91(1)	0.3306(9)	0.4809(1)	0.2500
					O2	6	0.96(1)	0.578(1)	0.460(1)	0.2500
					O3	12	0.902(9)	0.3422(7)	0.2579(8)	0.0722(8)
					P1	6	0.877(8)	0.3978(5)	0.3701(5)	0.2500
					Ca1	4	1	0.33333	0.66667	0.0019(7)
					Ca2	6	0.992(6)	0.2457(4)	0.9883(4)	0.2500
					O(H)	4	0.584(9)	0	0	0.172(2)
200°C/24 h	8.77	12.26	8.49	1.44	O1	6	0.92(1)	0.3299(9)	0.481(1)	0.2500
					O2	6	0.93(1)	0.581(1)	0.460(1)	0.2500
					O3	12	0.895(9)	0.3415(7)	0.2566 (8)	0.0707(8)
					P1	6	0.901(8)	0.3975(5)	0.3694(5)	0.2500
					Ca1	4	1	0.33333	0.66667	0.0018 (7)
					Ca2	6	0.998(6)	0.2462(4)	0.9896(4)	0.2500
					O(H)	4	0.5699(95)	0	0	0.179(2)
200°C/48 h	9.05	12.44	8.03	1.55	O1	6	0.939(9)	0.3290(8)	0.4788(9)	0.2500
					O2	6	0.97(1)	0.5810(9)		0.2500
					O3	12	0.872(8)	0.3394(7)	0.4622(9)	0.0736(7)
					P1	6	0.909(7)	0.3981(5)	0.2545(7)	0.2500
					Ca1	4	1	0.33333	0.3696(4)	0.0017(7)
					Ca2	6	0.999(5)	0.24547(3)	0.66667	0.2500
					O(H)	4	0.584(8)	0	0.9892(4)	0.182(2)
Holly Springs HAP					O1	6	1	0.3284(2)	0.4848(2)	0.2500
					O2	6	1	0.5873(2)	0.4651(2)	0.2500
					O3	12	1	0.3437(2)	0.2579(1)	0.0702(2)
					P1	6	1	0.3987(2)	0.3685(1)	0.2500
					Ca1	4	1	0.33333	0.66667	0.0015(1)
					Ca2	6	1	0.2468(2)	0.9934(2)	0.2468(2)
					O(H)	4	0.5	0	0	0.1950

The refinement was performed without incorporation of CO_3^{2-} ions in the Rietveld structural model

Table 4 Unit cell contents from Rietveld analyses

	200°C/4 h	200°C/8 h	200°C/24 h	200°C/48 h
Ca^{2+}	9.985(7)	9.953(8)	9.986(6)	9.996(5)
PO_4^{3-}	5.36(1)	5.262(8)	5.404(8)	5.455(8)
CO_3^{2-} [a]	0.64	0.738	0.596	0.545
O(H)	2.20(1)	2.33(1)	2.28(1)	2.33(1)
Ca/P	1.86	1.89	1.85	1.83

The refinement was performed without incorporation of CO_3^{2-} ions in the Rietveld refinement model

[a] The CO_3^{2-} content was evaluated as PO_4^{3-} and CO_3^{2-} is fixed at six

however, they became more intense with duration (Fig. 4c). The absence of structurally bounded OH^- (or its presence in very small amounts) in the most carbonated HAP has been reported in a very recent work [22].

3.4 Microstructure

The structure of cuttlefish bone is systematically and in detail described by Birchall et al. [19]. In short, it consists of two regions: a thick external wall or dorsal shield and internal regions with lamellae, which are separated by numerous pillars. In the internal matrix each of the

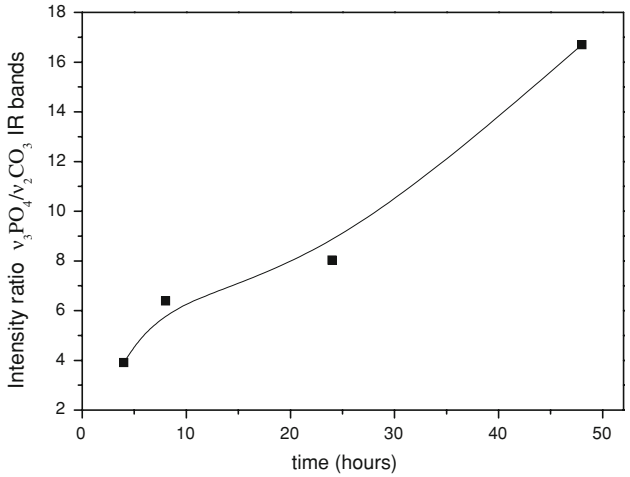

Fig. 5 Intensity ratio of v_3PO_4/v_2CO_3 IR bands versus time of HT treatment

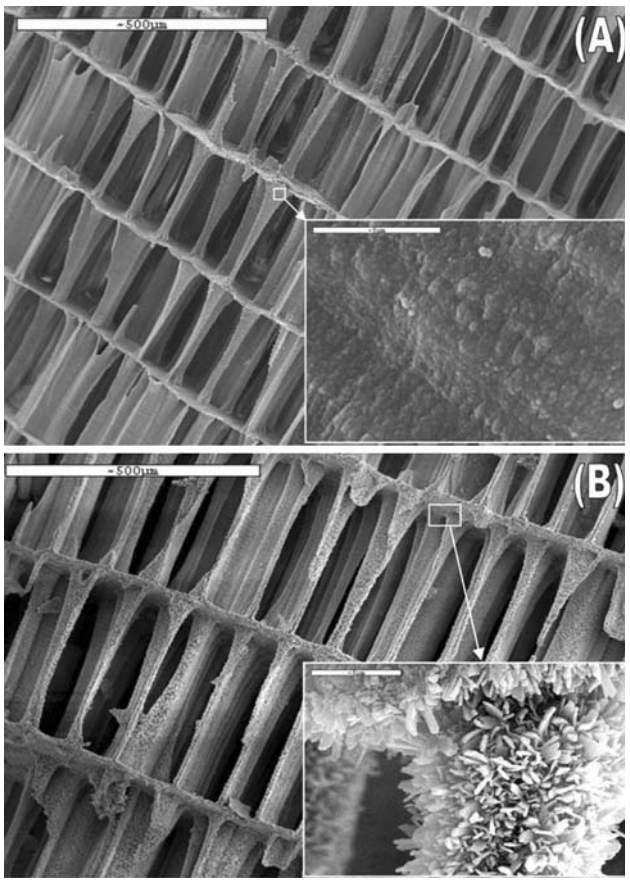

Fig. 6 SEM micrographs of: **a** cuttlefish bone heated at 350°C for 3 h. The corrugated appearance of the pillars is shown in the *inset*, **b** the cuttlefish bone after hydrothermal conversion at 200°C/24 h showing plate- and needle-like HAP crystals (*inset*)

individual lamellae and pillars are coated with organic material. The microstructure of cuttlefish bone hydrothermally converted into HAP is shown in Fig. 6. The same hollow interconnected structure of cuttlefish bone is retained during the HT conversion. As seen at higher magnification (inset in Fig. 6a), the corrugated appearance of pillars is characteristic for raw cuttlefish bone, while the transformed HAP shows plate- and needle-like HAP crystals. The HAP crystals are randomly oriented in the lamellae of the hydrothermally transformed cuttlefish bone (inset in Fig. 6b). This explains the increase of S_{BET} and total pore volume during the transformation, whereas the mean pore size does not change significantly (Table 1).

4 Conclusion

Hydrothermal transformation of aragonite ($CaCO_3$) from cuttlefish bone into HAP by treatment with $NH_4H_2PO_4$ at 200°C for various times (1–48 h) has been studied. The complete transformation of aragonite is achieved after 48 h. FT-IR spectra have shown the substitution of CO_3^{2-} predominantly in the PO_4^{3-} sites, but after 48 h HT treatment CO_3^{2-} were also found in small amounts in the OH^- sites of the structure. The FT-IR spectra and Rietveld refinement of HAP structure show subsequent incorporation of phosphate in the HAP structure with simultaneous decrease of CO_3^{2-} bands of the HAP structure. Hydrothermal conversion retains the interconnected channeled structure of cuttlefish bone while altering the chemical composition from aragonite to HAP. Plate- and needle-like crystals of HAP were formed. The specific surface area (S_{BET}) and total pore volume is increased and mean pore size somewhat decreased by HT treatment.

Acknowledgment The financial support of the Ministry of Science, Education and Sports of the Republic of Croatia in the framework of the project "Bioceramic, Polymer and Composite Nanostructured Materials", (No. 125-1252970-3005) and Universidad Politecnica de Valencia, (Centro de Biomateriales) Spain is gratefully acknowledged.

References

1. R.Z. Le Geros, in *Hydroxyapatite and Related Materials*, ed. by P.W. Brown, B. Constantz (CRC Press, Boca Raton, 1994), p. 3
2. D. Green, D. Walsh, S. Mann, R.O.C. Oreffo, Bone **30**, 810 (2002). doi:10.1016/S8756-3282(02)00727-5
3. R.M. Wilson, J.C. Elliot, S.E.P. Dowker, Am. Mineral. **84**, 1406 (1999)
4. J.C. Elliot, *Structure and Chemistry of the Apatites and Other Calcium Orthophosphates* (Elsevier, Amsterdam, 1994)
5. I.R. Gibson, W. Bonfield, J. Biomed. Mater. Res. **59**, 697 (2002). doi:10.1002/jbm.10044
6. T. Leventouri, Biomaterials **27**, 3339 (2006). doi:10.1016/j.biomaterials.2006.02.021
7. J. Hu, J.J. Russell, B. Ben Nissan, R. Vago, J. Mater. Lett. **20**, 85 (2001). doi:10.1023/A:1006735319725
8. Y. Xu, D. Wang, L. Yang, H. Tang, Mater. Charact. **47**, 83 (2001). doi:10.1016/S1044-5803(01)00154-1

9. K.S. Vecchio, X. Zhang, J.B. Massie, M. Wang, C.W. Kim, Acta Mater. **3**, 910 (2007)
10. R. Murugan, S. Ramakrishna, K. Panduranga Rao, Mater. Lett. **60**, 2844 (2006). doi:10.1016/j.matlet.2006.01.104
11. D.M. Roy, S.K. Linnehan, Nature **247**, 220 (1974). doi:10.1038/247220a0
12. M.S. Sivakumar, T.S. Sampath, K.L. Kumar, K. Shantha, K. Panduranga Rao, Biomaterials **17**, 1709 (1996). doi:10.1016/0142-9612(96)87651-4
13. C.H. Kasperk, R. Evers Zahnaertzl, Implant **2**, 234 (1986)
14. J.H.G. Rocha, A.F. Lemos, S. Agathopoulos, P. Valério, S. Kannan, F.N. Oktar, J.M.F. Ferreira, Bone **37**, 850 (2005). doi:10.1016/j.bone.2005.06.018
15. J.H.G. Rocha, A.F. Lemos, S. Agathopoulos, S. Kannan, P. Valerio, J.M.F. Ferreira, J. Biomed. Mater. Res. A **77**, 160 (2006). doi:10.1002/jbm.a.30566
16. R.A. Young, *The Rietveld Method, International Union of Crystallography, Monographs on Crystalography*, vol. 4 (Oxford Press, Oxford, 1993)
17. The software TOPAS V 2.1 of Bruker Advanced X-ray Solution, Bruker AXS, Karlsruhe, Germany (2003)
18. M.I. Kay, R.A. Young, A.S. Posner, Nature **204**, 1050 (1964). doi:10.1038/2041050a0
19. J.D. Birchall, N.L. Thomas, J. Mater. Sci. **18**, 2081 (1983). doi:10.1007/BF00555001
20. K. Sudarsanan, R.A. Young, Acta Crystallogr. B **25**, 1534 (1969). doi:10.1107/S0567740869004298
21. S. Chakraborty, S. Bag, S. Pal, A.K. Mukherjee, Appl. Crystallogr. **39**, 385 (2006). doi:10.1107/S0021889806010351
22. M.E. Fleet, X. Liu, Biomaterials **28**, 916 (2007). doi:10.1016/j.biomaterials.2006.11.003
23. A.F. Lemos, J.H.G. Rocha, S.S.F. Quaresma, S. Kannan, F.N. Oktar, S. Agathopoulos, J.M.F. Ferreira, J. Eur. Ceram. Soc. **26**, 3639 (2006). doi:10.1016/j.jeurceramsoc.2005.12.011
24. E. Landi, G. Celotti, G. Logroscino, A. Tampieri, J. Eur. Ceram. Soc. **23**, 2931 (2003). doi:10.1016/S0955-2219(03)00304-2
25. H.L. Feki, J.M.A. Savariault, A. Ben Salah, J. Alloy. Compd. **287**, 114 (1999). doi:10.1016/S0925-8388(99)00070-5